# ON THE MODELING OF LEFT ATRIAL APPENDAGE INVERSION: A REVERSE GROWTH ANALYSIS

# R. SCUOPPO[*], AND S. PASTA[†]

[*] Department of Engineering, Università degli Studi di Palermo, 90128 Palermo, Italy
e-mail: roberta.scuoppo@unipa.it
[†] Department of Engineering, Università degli Studi di Palermo, 90128 Palermo, Italy
e-mail: salvatore.pasta@unipa.it

**Key words:** Atrial Fibrillation, Left atrial appendage, Finite element method, Reverse growth.

**Abstract.** Atrial fibrillation (AF) can lead to thromboembolic events due to an increased propensity for clot formation in the left atrial appendage (LAA). Current methods for reducing the risk of these events, such as surgical exclusion and percutaneous occlusion, have limitations that restrict their applicability and efficacy. Sulkin et al. [1] previously demonstrated the clinical feasibility of a novel procedure involving partial inversion of the LAA to occlude the atrium appendage.

This study aimed to explore left atrial appendage inversion (LAAI) on four patient-specific LAA morphologies, each representing a distinct morphological variant: chicken wing, cactus, windsock, and cauliflower. Left atrial geometries were extracted from CT images and then used as input for patient-specific finite element analysis simulations of LAAI. The latter was simulated by pulling the elements at the LAA tip along a predefined path to mimic the inversion. The deformed configuration was then analyzed to map the stress field and establish a stress-resorption relationship.

Folded LAA wall results in a transition from tensile to compressive stress distribution, which can induce tissue resorption in the inverted appendage. This compressive stress distribution is linked to the stretch distribution ($\lambda$) generated in the folded LAA. To define a stress-resorption relationship, the growth and reverse growth kinematics proposed by Lee et al. [2] was adopted. This approach involves a reversible growth multiplier ($\theta$) that represents the combined effects of elastic deformation and tissue growth/reverse growth., The trend of $\theta$ based on the strain-driven growth model was derived using the Ogden constitutive model. The value of $\theta$ depended to $\lambda$, and tissue resorption was triggered beyond a stretch threshold. Thus, we concluded that $\lambda$ generated in the LAAI region acts as a remodeling stimulator. This occurred until $\lambda$ decrease below a minimum value and $\theta$ converged to a final value following an exponential decay trend. Our findings resulted in a stress-growth model, applied in four LAA morphologies, that can model tissue resorption over time as compressive tensile gradually relax in the inverted LAA.

# 1 INTRODUCTION

Atrial fibrillation (AF) is the most common arrhythmia encountered in clinical practice, with a pooled incidence in community-based studies averaging 4.70 per 1000 person-years, and a prevalence ranging from 2% in people < 65 years to 9% in those > 65 years and almost 18% in the elderly (> 85 years) [3]. The condition is particularly critical because AF increases the risk of stroke fivefold, with stroke being the second leading cause of death and the primary cause of disability among adult-elderly individuals [4]. The management of AF and associated complications imposes substantial economic burdens on healthcare systems, with annual costs running into billions of dollars.

According to the guidelines of the European Society of Cardiology, stroke prevention in AF patients is paramount, and oral anticoagulants are recommended for most patients [5]. However, oral anticoagulants require continuous monitoring and come with significant bleeding risks, particularly in elderly patients or those with concomitant illnesses. These guidelines also highlight the potential for left atrial appendage (LAA) occlusion as an alternative for patients who have contraindications to long-term anticoagulation therapy.

The LAA is the primary site where thrombi form in AF patients, leading to embolic events. Current LAA closure techniques involve the use of various devices and surgical methods to occlude or exclude the appendage permanently. However, percutaneous approaches can be complicated by device migration, incomplete closure, and potential thromboembolic events.

To address these limitations, a novel technique was developed to partially invert the LAA into the left atrium [6], leveraging the natural tissue response mechanisms of the cardiac tissue to achieve occlusion without leaving any permanent implants. The LAAI procedure is designed to induce compressive stresses within the inverted tissue, promoting gradual resorption and eventual occlusion over time. This approach not only aims to reduce the risks associated with permanent devices but also utilizes the heart tissue remodeling capability [7].

This study presents a comprehensive computational framework to simulate the LAAI procedure across different LAA morphologies, categorized as chicken wing, windsock, cactus, and cauliflower. Utilizing patient-specific anatomical models derived from CT imaging, finite element analyses were performed to understand the biomechanical behavior during and after inversion. Simulations were based on the Ogden hyperelastic material model to represent the left atrial tissue and incorporate a stress-resorption law to predict reverse growth. Findings provided novel insights into the potential of LAAI as a minimally invasive, device-free alternative for stroke prevention in AF patients. A comparison of LAAI procedures among various LAA morphologies was assessed.

# 2 MATERIALS AND METHODS

## 2.1 Patient-specific LAA modeling

A retrospective analysis was performed to identify four patients with AF and different LAA morphological variants. These were the chicken wing, windsock, cactus, and cauliflower morphologies. For each patient, the ECG-gated CT images were processed in Mimics (v.21, Materialize, Belgium) to reconstruct the geometry of left atrium (LA), including LAA. This involved semi-automatic thresholding of contrast-enhanced images, followed by manual editing, and smoothing [8]. Thus, the four LA were exported as an STL file for further

processing in Rhinoceros software (v.7, McNeel & Associates, USA). The left atrial geometries had four inlets (pulmonary veins) and one outlet (mitral valve) that were cuts using perpendicular planes to achieve a regular patient geometry. The centerline of each LAA was reconstructed and then used to drive the direction of LAAI procedure in the structural simulations.

Each anatomical part was meshed using ICEM meshing software (v2021, ANSYS Inc., USA) following a convergence analysis. The discretization error was kept below 1%, using the maximum principal stress as the output for comparison among different grid sizes. Consequently, the patient-specific LAA model was meshed with unstructured triangular shell elements, with an element size of 1.2 mm for the atrium and 0.6 mm for the LAA, to ensure adequate resolution for subsequent simulations.

## 2.2 LAAI finite element analysis

The biomechanical behavior of the LA tissue wall was assumed as a hyperelastic and isotropic material using a third-order Ogden's strain energy function:

$$W = \sum_{i=1}^{3} \frac{\mu_i}{\alpha_i} (\lambda_1^{\alpha_i} + \lambda_2^{\alpha_i} + \lambda_3^{\alpha_i} - 3) \qquad (1)$$

This function incorporates three pairs of material parameters ($\mu_i$, $\alpha_i$) to describe the principal stretches ($\lambda i$). Specifically, the material parameters were: $\mu_1 = 56.13$ MPa, $\alpha_1 = 8.65$, $\mu_2 = 42.88$ MPa, $\alpha_2 = 10.03$, $\mu_3 = 13.59$ MPa, and $\alpha_3 = 6.82$ [6]. To simulate the LAAI procedure, the catheter clamping of the LAA was first simulated by constraining the element nodes at the distal apex of the LAA. Subsequently, the inversion was simulated by pulling the clamped elements inside the heart along the LAA centerline obtained in Mimics. This motion was implemented through connector assignments of constrained nodes in the ABAQUS commercial software (ABAQUS v2020, Dassault Systèmes, Waltham, MA, USA). A velocity boundary condition along the centerline direction was applied to the control central point of the connector to complete the inversion of the distal portion of the LAA, thereby mimicking the LAAI procedure.

Boundary conditions were applied to fix the distal ends of the pulmonary veins and mitral valve in all directions. A hydrostatic pressure of 1 mmHg at the inner left atrial surface was used to account for blood pressure. The general contact algorithm with frictionless conditions was adopted to consider the interaction of the LAA tissue wall with itself during the LAAI simulation. The ABAQUS/Explicit solver was used to consider the simulation nonlinearity including large deformation and complex contact conditions. Energy monitoring was employed to ensure the ratio of kinetic energy to internal energy remained below 10%, and a variable mass-scaling technique was adopted to maintain the time step below $10^6$. Post-processing was performed using Ensight software.

## 2.3 Reverse growth kinematics

In biological materials, the deformation gradient can be decomposed into two distinct parts: one representing the growth of the tissue (Fg) and the other accounting for the shape changes due to applied stresses (Fe). Thus, the deformation gradient can be broken up into an elastic and a plastic part [7, 9]. A growth and remodeling equation was required to understand the

relationship between the deformation rate due to growth and the current stress state of the material. This equation enables the capture of how the growth process is influenced by the stress within the tissue.

The model here used is based on the generic framework of volumetric strain-driven finite growth described by Göktepe et al. This model is based on the formulation of a reversible growth multiplier θ and its constitutive modeling by using an isotropic growth tensor Fg:

$$Fg = \theta\, I \qquad (2)$$

$$\frac{d\theta}{dt} = k(\theta)\phi(\lambda e)$$

In Eq. (2), the evolution of the growth multiplier depended on two scalar functions, namely, a rate limiting scalar function $k(\theta)$ and a growth driving function $\phi(\lambda e)$ that depends on the elastic myofiber stretch $\lambda e$.

$$k(\theta) = \frac{1}{\tau_g}\left(\frac{\theta_{max} - \theta}{\theta_{max} - \theta_{min}}\right)^{\gamma_g} \qquad (3)$$

$$\phi(\lambda e) = \lambda e - \lambda_{h_2}$$

In this Eq. (3), $\gamma_g$, $\tau_g$, $\theta_{max}$ and $\theta_{min}$ were the degree of nonlinearity of myofiber, a timescale associated with tissue growth and the prescribed maximum and minimum permissible values of the growth multiplier θ, respectively. $\lambda e$ is the elastic myofiber stretch. It is evident from Eq. (3) that growth terminated when either criterion $\theta = \theta_{max}$ or $\lambda e = \lambda_{h2}$ is met.

Lee et al [2] hypothesized that cardiac growth is reversible in a way that the elastic myocardial stretch $\lambda e$ is always normalized to a homeostatic range $\lambda_{h1} \leq \lambda e \leq \lambda_{h2}$. Consequently, reverse growth occurs when the elastic myofiber stretch is less than the prescribed homeostatic myofiber stretch $\lambda_{h1}$. To model reversible growth, Eq. 3 assumed the following functional forms for $k(\theta)$ and $\phi(\lambda e)$ when $\lambda e \leq \lambda_{h1}$:

$$k(\theta) = \frac{1}{\tau_{rg}}\left(\frac{\theta - \theta_{min}}{\theta_{max} - \theta_{min}}\right)^{\gamma_{rg}} \qquad (4)$$

$$\phi(\lambda e) = \lambda e - \lambda_{h_1}$$

Reversal of growth terminated when either criterion: $\theta = \theta_{min}$ ($\theta_{min} > 0$) or $\lambda e = \lambda_{h1}$ were met. To ensure that growth does not occur within the homeostatic range of the elastic myofiber stretch, we prescribed $\phi = 0$ when $\lambda_{h1} \leq \lambda e \leq \lambda_{h2}$. For the growth parameters, $\tau_{rg} = 1$, $\gamma_{rg} = 1$ and $\lambda_{h1} = 1.15$ were chosen.

Pressure-time variations were prescribed to simulate stretch-driven reverse growth. A cyclical low end-diastolic pressure of 10 cycles (P = 2 mmHg) was applied successively to induce stretch-driven reverse growth. Figure 1 shows the trend of the scalar function $k(\theta)$. In this study, the timescale of a cardiac cycle and the timescales of reverse growth were separated each other. Thus, the growth multiplier θ was updated only at peak pressure in each cycle. In particularly, we update the colored map of θ at the end of the first pressure cycle, at the fifth pressure cycle and at the last one, when $\lambda e$ reaches the threshold value that stops reverse growth. Simulations of cyclical pressure were conducted using the ABAQUS/Explicit solver, while the evaluation of reverse growth multiplier was performed using Ensight software.

## 3   RESULTS

Figure 2A shows the segmentation of the left atrium for the chicken wing morphology while the Figure 2B illustrates the other auricle shapes for the four patients included in this study. The difference in the auricle morphologies can be observed.

Figure 3 illustrates the deformed shapes of the partial inversion of each auricle across the four morphological variants. When LAAI is compared with the undeformed shape, the resulting inversion had difference from patient-to-patient according to the auricle morphology. The windsock morphology exhibited slight folding due to a pronounced extension and thin geometry, which led challenges in the simulation solution. The choice of velocity direction at the tip of the LAA facilitated the inversion of geometries and prevented folding or overlapping of the element mesh.

Figure 4 displays the evolution of the maximum principal stress at LAAI tip over time. It is noteworthy that all geometries exhibit a compressive stress state in the folded LA during the inversion process. The peak compressive stress was -3.9 MPa for the windsock-related LAAI while the cactus-type LAAI exhibited a remarkable positive stress of 4.2 MPa before inversion.

Figure 5 illustrates colored stress maps representing the stress distribution at 50% and 100% of LAAI procedure:

- At 50% inversion, the stress distribution provides insights into the initial response of the geometry to the inversion process. Variations in stress intensity and distribution can be observed across different morphologies;
- Upon reaching 100% inversion, the stress maps reveal the final stress distribution. The blue negative areas, characterized by compressive stress, mark the starting points for simulating the process of reverse growth to occlude the LAA.

The cactus morphology exhibits a different pattern of appendage inversion as compared to other auricle morphologies, with negative pressure generated within the atrial portion of the inverted region.

Figure 6 shows the remodeling stress map on each LAAI simulation as represented by the reverse growth multiplier ($\theta$). The magnitudes of $\theta$ parameter were mapped at the end of the first pressure cycle, the fifth pressure cycle and the tenth pressure cycle. Theta values are highest in regions corresponding to the negative pressure generated within the folded portion of LAA, reaching maxima of 0.4 at the first peak pressure, where the reverse growth process initiates. In a different way, theta is lowest in regions experiencing positive pressure and decreases with increasing pressure cycles. The reverse growth process stops when $\lambda e$ is equal to $\lambda_{h1}$. These maps of reverse growth multiplier exhibited the spatiotemporal distribution of reverse growth for each LAAI.

## 4   DISCUSSIONS AND CONCLUSIONS

Using patient-specific geometries, the LAAI procedure was simulated for four LAA morphologies by applying velocity boundary conditions along the auricle centerline to pull the LAA tip. This study provides insights into the biomechanical response of the LAAI procedure, including remodeling simulations to evaluate the long-term efficacy for stroke prevention in patients with AF.

The study demonstrated that the inversion procedure can lead to compressive stress in the folded zone upon peaks of nearly -0.4 MPa for all LAAI simulations. A stress-growth model

was adopted to simulate the reverse growth induced by the compressive stress field in the inverted tissue portion. We observed the gradual relaxation of compressive stresses within the inverted appendage towards tissue resorption over time. This likely suggests occlusion of the atrial appendage by inversion.

Current LAA closure approaches with epicardial and endocardial devices rely on a permanent implantation of the device in the repaired appendage. This permanence can lead to complications such as LAA perforation, migration, incomplete closure, new thrombus formation and thromboembolic events. The LAAI concept proposed here promotes resorption without requiring permanent devices or implants [10]. It is mentioned that the partial inversion of LAAI is clinical preserved with the utilize of tissue glue to keep the auricle at inverted stage.

The generation of compressive stresses occurred when tissue stretches deviated from homeostatic thresholds. The adopted reverse growth model calculated a growth multiplier using the principal stretch. Reverse growth was assumed to initiate when the stretches generated by the inverted portion of the auricle were lower than the homeostatic stretch values [11]. Mechanobiological control mechanisms in the myocardial wall tend to restore strain values toward preferred homeostatic values in response to various alteration from normal conditions. Under low-pressure cyclical loads, the gradual relaxation of stress was associated with a reduction of the growth multiplier over time until the stretch values returned to the homeostatic value of 1.15. The latter was the condition for which the reverse growth process stopped. Though this approach provided valuable mechanistic insights in the LAAI, validation studies are warranted to confirm the accuracy and predictive capabilities of current findings.

There are several limits to the present study. The left atrium was assumed as a passive and isotropic material with uniform thickness and not any myofiber-related orientation. Such assumptions may have influenced the resulting inversion morphologies and stress-growth distributions. Moreover, the trend of the growth multiplier was mapped a posteriori on the geometry of the LAA without considering the alterations in shape and material properties that occur during remodeling. To address these limitations, we are developing an Abaqus-explicit subroutine (VUMAT) as done by Young et al. [12]. This subroutine should integrate the material model with the growth model, to achieve an accurate representation of the LAAI mechanobiology. The approach should be based on a decomposition of the strain gradient into an elastic part and a growth part, allowing for real-time adjustments to the geometry and material properties of the LAA during remodeling.

Fluid-solid interaction (FSI) analysis could provide additional information on the risk of thrombus formation in the inverted appendage [13]. FSI analyses can enable the assessment of the dynamic interactions between blood flow and tissue mechanics within the LAA, providing insights into hemodynamic changes post-inversion. In this context, Musotto et al. [13] developed an electro-mechanical coupling analysis to mimic left atrium contraction by applying a thermal load on the LAA wall. Their study highlighted the thrombus risk associated with different AF conditions and LAA shapes. Currently, we are performing FSI simulations of LAAI procedures to quantify the risk of thrombosis based at different stages of LAAI remodeling. These simulations are expected to provide in the mechanistic link between LAA morphology and inversion-induced tissue remodeling [14, 15].

This study provided valuable insights into the efficacy of LAAI for stroke prevention in AF patients and elucidated the procedure feasibility across different LAA morphologies. The stress-driven reverse growth model offered an understanding of the long-term response after

LAAI, highlighting differences across various appendage morphologies.

# REFERENCES

1. Sulkin, M.S., et al., *Suction catheter for enhanced control and accuracy of transseptal access.* EuroIntervention, 2016. **12**(12): p. 1534-1541.
2. Lee, L.C., et al., *A computational model that predicts reverse growth in response to mechanical unloading.* Biomechanics and Modeling in Mechanobiology, 2015. **14**(2): p. 217-229.
3. Kornej, J., et al., *Epidemiology of Atrial Fibrillation in the 21st Century: Novel Methods and New Insights.* Circ Res, 2020. **127**(1): p. 4-20.
4. Escudero-Martinez, I., L. Morales-Caba, and T. Segura, *Atrial fibrillation and stroke: A review and new insights.* Trends Cardiovasc Med, 2023. **33**(1): p. 23-29.
5. Hindricks, G., et al., *2020 ESC Guidelines for the diagnosis and management of atrial fibrillation developed in collaboration with the European Association for Cardio-Thoracic Surgery (EACTS): The Task Force for the diagnosis and management of atrial fibrillation of the European Society of Cardiology (ESC) Developed with the special contribution of the European Heart Rhythm Association (EHRA) of the ESC.* Eur Heart J, 2021. **42**(5): p. 373-498.
6. Pasta, S., J.M. Guccione, and G.S. Kassab, *Inversion of Left Atrial Appendage Will Cause Compressive Stresses in the Tissue: Simulation Study of Potential Therapy.* J Pers Med, 2022. **12**(6).
7. Guccione, J.M., et al., *Residual stress produced by ventricular volume reduction surgery has little effect on ventricular function and mechanics: A finite element model study.* Journal of Thoracic and Cardiovascular Surgery, 2001. **122**(3): p. 592-599.
8. Scardulla, F., et al., *Shear stress alterations in the celiac trunk of patients with a continuous-flow left ventricular assist device as shown by in-silico and in-vitro flow analyses.* J Heart Lung Transplant, 2017. **36**(8): p. 906-913.
9. Klepach, D., et al., *Growth and remodeling of the left ventricle: A case study of myocardial infarction and surgical ventricular restoration.* Mechanics Research Communications, 2012. **42**: p. 134-141.
10. Lorenzoni, G., et al., *Percutaneous Management of Left Atrial Appendage Perforation: Keep Calm and Think Fast.* J Invasive Cardiol, 2018. **30**(11): p. E126-E127.
11. Omens, J.H., *Stress and strain as regulators of myocardial growth.* Progress in Biophysics & Molecular Biology, 1998. **69**(2-3): p. 559-572.
12. Young, J.M., et al., *Automatic Generation of User Material Subroutines for Biomechanical Growth Analysis.* Journal of Biomechanical Engineering-Transactions of the Asme, 2010. **132**(10).
13. Musotto, G., et al., *The Role of Patient-Specific Morphological Features of the Left Atrial Appendage on the Thromboembolic Risk Under Atrial Fibrillation.* Frontiers in Cardiovascular Medicine, 2022. **9**.
14. Garcia-Villalba, M., et al., *Demonstration of Patient-Specific Simulations to Assess Left Atrial Appendage Thrombogenesis Risk.* Front Physiol, 2021. **12**: p. 596596.
15. Masci, A., et al., *The Impact of Left Atrium Appendage Morphology on Stroke Risk Assessment in Atrial Fibrillation: A Computational Fluid Dynamics Study.* Front Physiol, 2018. **9**: p. 1938.
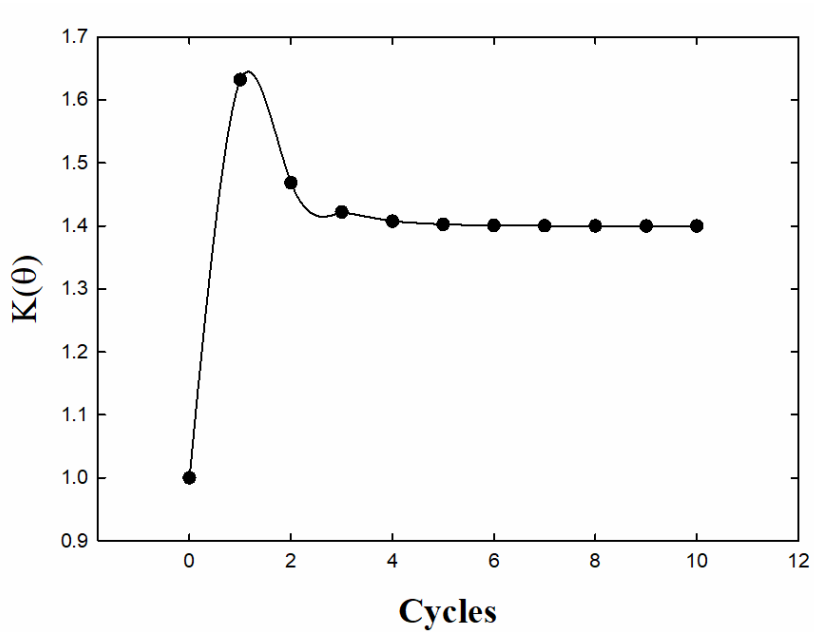
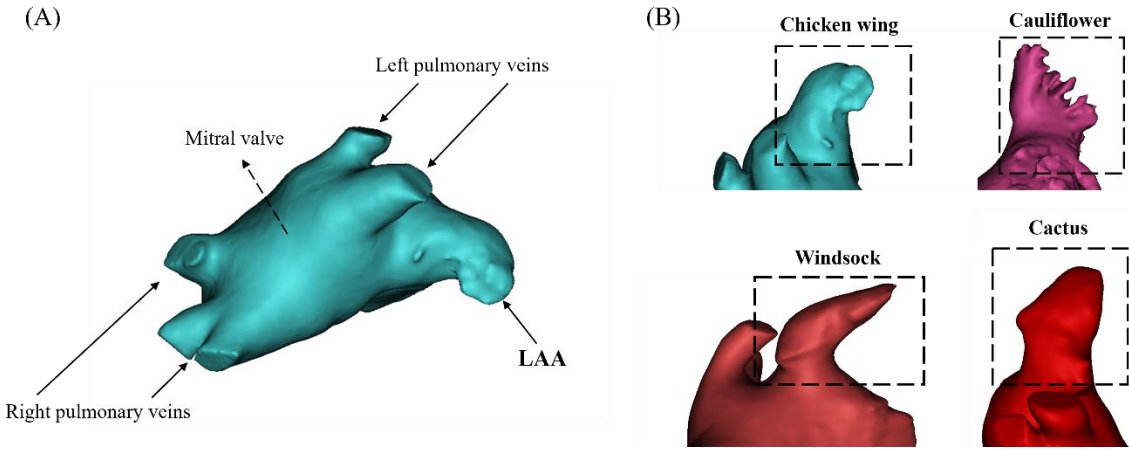**Figure 1**: Trend of the scalar function k(θ) during the 10 pressure cycles.



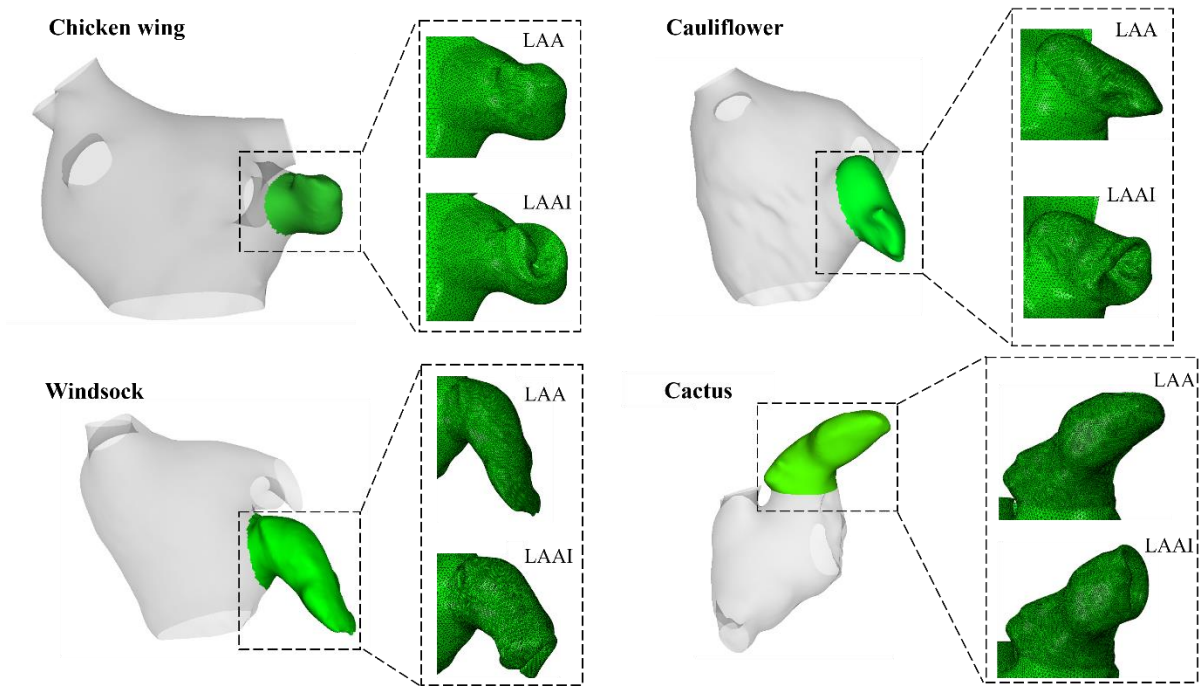**Figure 2**: (A) Segmented chicken wing LAA; (B) Four segmented LAA morphologies.

**Figure 3**: Finite element analysis of LAAI in the four morphologies, comparison between initial configuration and final folded configuration.
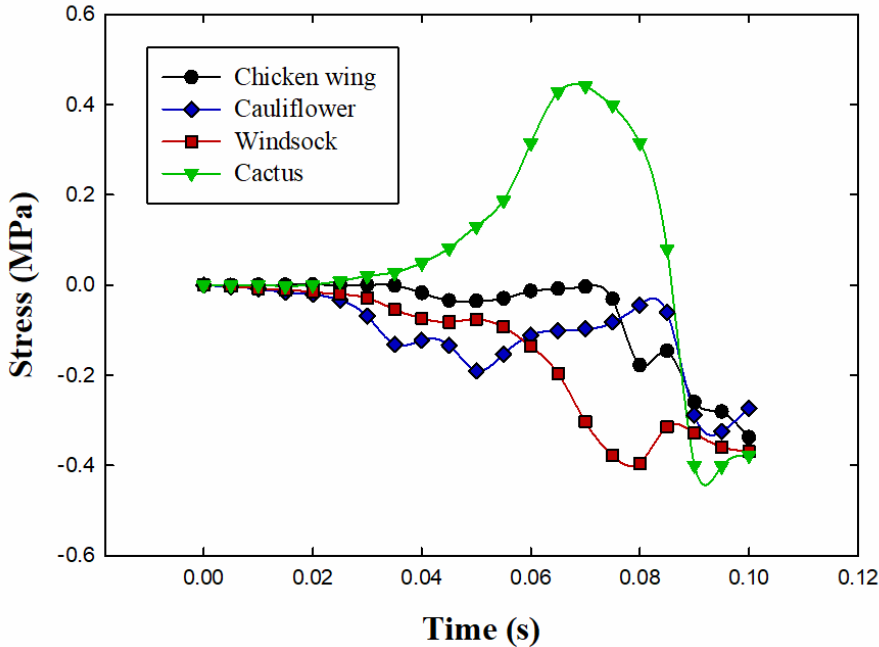


**Figure 4**: Stress trend during the LAAI simulation for the four morphologies in an element located in the folded LAA region.
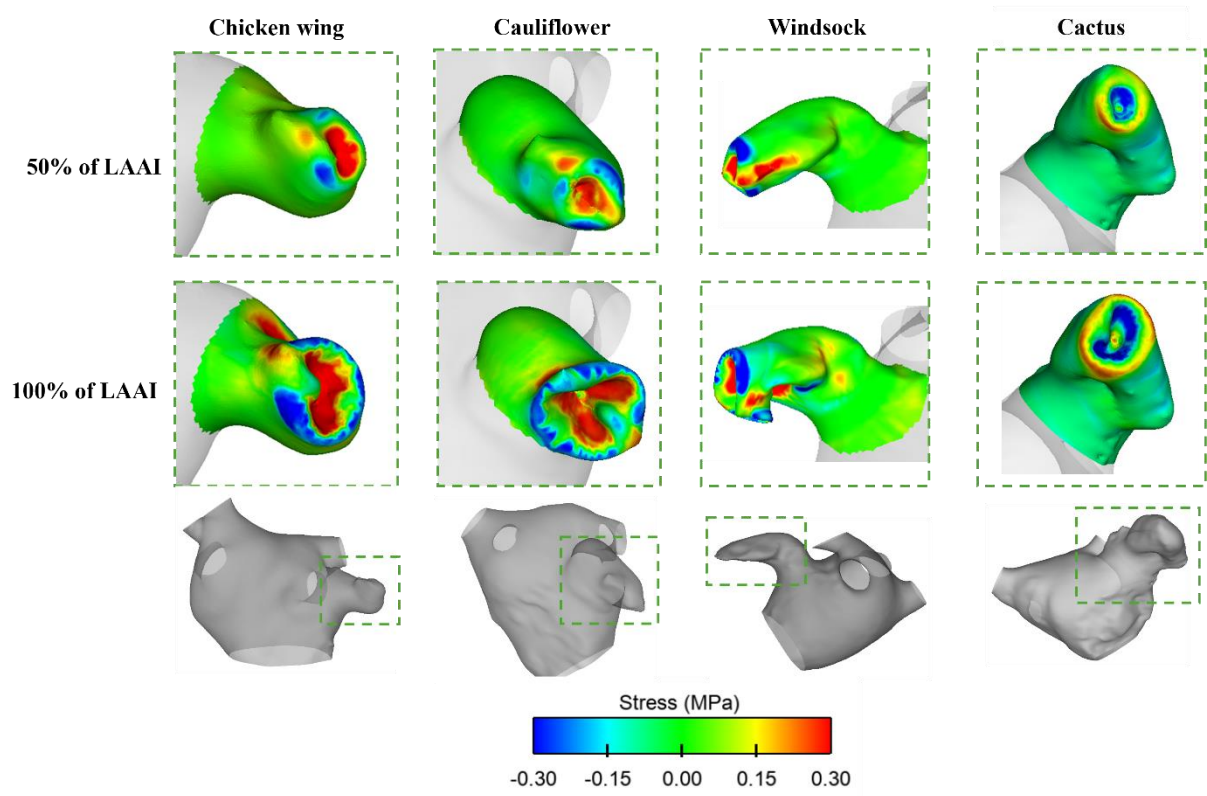
**Figure 5**: Colored map of compressive stress generation in 50% of LAAI and 100% of LAAI for chicken wing, cauliflower, windsock, and cactus geometries.
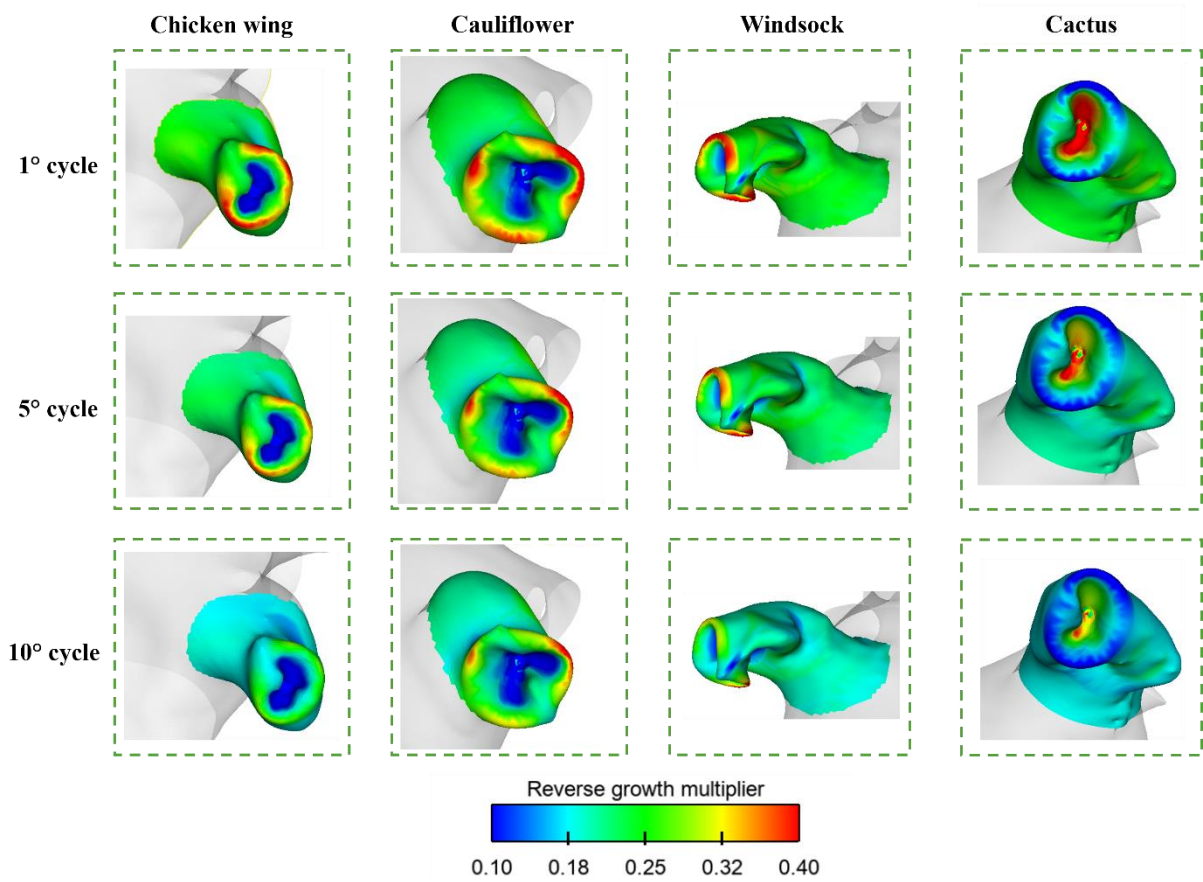
**Figure 6**: Colored map of reverse growth multiplier at the peak of 1° cycle, 5° cycle and 10° cycle for chicken wing, cauliflower, windsock, and cactus geometries.